Dil [22] (dilatometrische Daten ε_D - 5%)

Valery A. Udovenko, Pavel L. Potapov*, Natalia A. Poliakova* and Viktor Prieb***

(Institute of Physical Metallurgy, 2nd Baumanskaya, 9/23, 007005 Moscow, Russia; ** Berlin Technical University, Str. des 17. Juni 135, D-10623 Berlin, Germany)*

Martensitic Transformation in Antiferromagnetic Alloys of NiMn Intermetallic Compound

Using X-ray and neutron diffraction analysis, transmission electron microscopy, dilatometry and magnetic susceptibility measurements, the crystalline and magnetic structures in the NiMn intermetallic compound alloyed with Ti were studied. It is shown that the driving force for the martensitic transformation is of non-magnetic nature.

1 Introduction

Recently, considerable attention has been devoted to investigations of the thermoelastic martensitic transformations in the Cu-based alloys. It has been found that some unusual mechanical, elastic and thermal properties of these alloys are closely related with thermoelasticity first observed by Kurdjumov and Khandros in 1949 [1]. The thermoelasticity phenomenon is well known in ordered alloys with B2 structure: CuZn, AuCd, NiTi, NiAl, etc. [2 to 4]. These alloys undergo a Zener-type transition from the soft bcc structure with high frequency entropy to the low energetic close packed structure at temperatures usually exceeding 400 K.

In contrast, the transformation in some B2 ordered Mn-based alloys with Au, Pd, Pt, Ir, Ni seems to be more complicated [5 to 9]. In these intermetallic compounds antiferromagnetic ordering is accompanied by a tetragonal distortion of the parent cubic structure. So the transformation from the high temperature B2 structure to the low temperature $L1_0$ structure is observed in the vicinity of the Neel point (T_N). As a rule, the T_N value is high in these alloys and can vary from 500 K in MnAu [8] to 1000 K in NiMn [7]. The tetragonal distortions in these alloys are also high and can reach 5 to 6 %. These distortions are believed to be attributable to a reversible phase transition of the martensitic type [7, 8]. This mechanism was reported for disordered Mn (Ni, Cu, Ga, Ge) alloys with fcc/fct transformation [10]. However, the mechanism of transformation in intermetallic compounds exhibiting antiferromagnetism is uncertain at present because systematic examination of dependable crystalline and magnetic structure data combined with magnetic property anomalies is missing. This work presents such a study.

NiMn was chosen because antiferromagnetic interactions are most pronounced in this intermetallic compound. The high transformation temperature of this alloy, however, is not favourable for the experimental procedures but it decreases by Ti, Al, V, Cr additions [11]. NiMn was alloyed by Ti in the present work. In addition, alloying of NiMn can lead to a modification of the tetragonal $L1_0$ martensitic structure to a more complex monoclinic one [12]. Therefore, the correlation between crystalline and magnetic structures is important for an understanding of the nature of the transformation.

2 Experimental Methods

Alloys were prepared by induction melting in an argon atmosphere, starting from high purity materials. The chemical compositions in the present work are denoted in at.%. The ingots were homogenized at 1173 K in an evacuated tube during 10 h and water quenched.

Dilatometer measurements of rectangular slabs of a size of about 1 mm × 4 mm × 20 mm were carried out at a rate of 10 K/min during heating and cooling. X-ray and neutron scattering measurements were performed using powder specimens. The X-ray diffraction study was made using Fe-Kα radiation. Neutron scattering measurements were performed using a Curran diffractometer at a 10 MW research reactor in Karpov's Institute of Physic and Chemistry in Obninsk (Russia). A Pb monochromator was used to select a neutron wavelength of 0.128 nm. The powder specimens were enclosed in a thin-walled Ti–Zr can of 10 mm diameter. The composition of Ti–Zr alloys was close to a so-called "zero-matrix" which does not show fundamental Bragg peaks because the scattering lengths of Ti and Zr are similar in absolute value and opposite in sign. Transmission electron microscopy (TEM) investigations were carried out using a TESLA BS-540 electron microscope operated at 120 kV.

The static susceptibility was determined using a Faraday method at applied fields up to 8 kOe. The susceptibility as a function of temperature of quenched specimens (3 mm in diameter, 5 mm long) was measured first during cooling from room temperature to 15 K, then during heating from 15 to 500 K. Measurements were performed in a cryostat under flowing helium vapour at low temperatures and in an electric microfurnace with an argon atmosphere to prevent oxidation at high temperatures. The rates of heating and cooling were equal to 5 K/min.

3 Structure

To study the alloying effect on the NiMn structure three different types of Ti additions were used: substituting for both Ni and Mn with Ti, substituting for Ni with Ti, substituting for Mn with Ti but not verified on the atomic scale (based on stoichiometric balances of the sublattices). In all cases, alloying of NiMn by Ti leads to remarkable changes in the X-ray diffraction pattern.

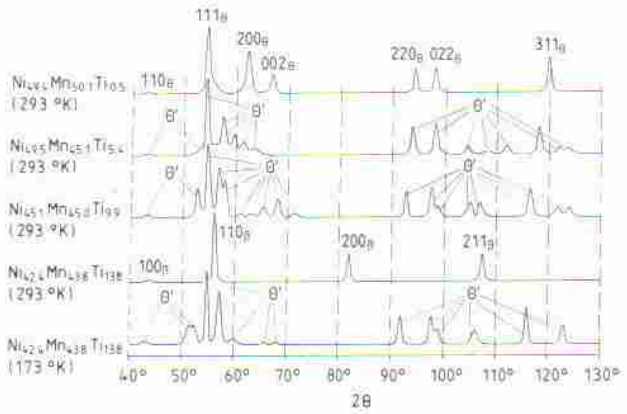

Fig. 1. X-ray powder diffraction profiles for NiMn(Ti) alloys (see text for details).

Figure 1 presents the diffraction pattern for NiMn(Ti) alloys with nearly equal Mn and Ni content. Like equiatomic NiMn, NiMn(Ti) containing 0.5 % Ti shows fct structure with some asymmetric diffuse broadening of the (200) and (111) peaks. With increasing Ti content the (111) and (110) reflections remain essentially unchanged but the (220), (022) and (311) angular positions shift. At the same time the (200) and (002) peaks disappear and a number of additional peaks appear in the 50 to 70° and 100 to 120° ranges of 2Θ. Thus the θ structure of NiMn martensite is modified by Ti addition although some symmetry elements of the initial structure are inherited. The modified structure of NiMn(Ti) is called θ' in the present work. The θ' diffraction pattern is observed with only small variations in NiMn(Ti) containing 5 to 15 % Ti. If the Ti content exceeds 15 %, the θ' diffraction pattern is substituted for the bcc one, containing weak (100) superstructural reflections indicating that the bcc structure is ordered. Thus the $\beta \rightarrow \theta'$ transformation in the alloys containing 15 % Ti seems to take place below room temperature. This was directly proved by an X-ray study at 173 K (see Fig. 1). A diffraction profile of the θ' phase similar to that observed in (5 to 15) % Ti alloys was found after cooling. After heating to room temperature the β pattern was fully restored. This indicates that $\beta \rightarrow \theta'$ as well as reverse $\theta' \rightarrow \beta$ transformation are of martensitic type.

The diffraction patterns of the θ' and β phases in alloys with constant Mn content (when Ti replaces Ni) exhibit a behaviour close to that described above. The θ' pattern is substituted for the β NiMn(Ti) one at a Ti concentration of about 12 %. In addition, the (200), (220) and (311) peaks of the fcc structure with $a = 0.3855$ nm have been found in $Ni_{50-x}Mn_{50}Ti_x$ alloys with $x = (5$ to $12)$. Taking into consideration that these alloys contain a lot of manganese, the fcc phase is probably γ-Mn related. To prove this hypothesis alloys with Mn contents between 52 and 55 % were additionally examined. The intensity of the fcc (220) peak in comparison with 0' peaks has been found to increase with increasing Mn content. The effect is similar but not so pronounced when the Ti content increases. This is in good agreement with the supposition that the γ phase in the alloys is Mn-based. In the alloys with $x = (12$ to $15)$, the γ phase coexists with β-NiMn(Ti). If $x = (12$ to $15)$, the γ phase pattern is substituted for another complicated diffraction profile. Analysis of the angular positions and intensities of the peaks shows that the structure is C19 with lattice parameters close to the ones in the intermetallic compound Mn_2Ti [13]. So the alloys in this composition range possess a heterophase structure in which NiMn(Ti) (in θ' or β allotropic forms) can coexist with the γ phase or with the Mn_2Ti intermetallic compound.

The behaviour of the alloys where Ti replaces Mn (with constant Ni content) is the same as described above. These alloys exhibit heterophase structures too, but the second phase was identified as Ni_3Ti.

As heterophase alloys are not interesting for the present work, we will concentrate mainly on homogeneous alloys. The β- and θ-NiMn(Ti) structures will now be described in more detail. For the $L1_0$ structure, the (111) peak represents diffraction from close packed (basal) planes; (220) and (022) peaks refer to planes which are perpendicular to basal planes. As these peaks remain unchanged upon alloying (see Fig. 1), the θ' structure is believed to possess the same basal planes as θ-NiMn. On the other hand, the (200) and (022) peaks correspond to planes tilted from {111} by about 55°. Thus the intensities of these peaks depend strongly on the stacking sequence of the basal planes. In the $L1_0$ structure it is ABCABC... . It can be supposed that the stacking sequence in NiMn(Ti) exhibits another type. This supposition is confirmed by TEM examination. Figure 2 shows TEM diffraction patterns for NiMn(Ti) with various Ti concentrations. There are extra reflections along the ⟨111⟩ direction which divide the ⟨111⟩ distance into 8, 5, 4 equal parts in alloys containing 5.4, 7.8, 9.8 % Ti, respectively. So the period of atomic layer stacking seems to be 8, 5 and 4 layers depending on the Ti content.

On the basis of these TEM results the X-ray profiles of a θ-NiMn(Ti) may be fully interpreted. Let us consider the $NiMn_{40.2}Ti_{9.8}$ alloy, for instance. It is useful to assume the orthorhombic unit cell (Fig. 3). The lattice parameters a, b, c/L (parameter c is determined through L, the number of atomic layers in the cell) can be calculated as 0.4417, 0.2679, 0.2134 nm, respectively, from the 2Θ positions of the (222), (220) and (022) peaks in $L1_0$ terms. In terms of the orthorhombic cell these peaks are (00.2L), (02.0) and (31.0), respectively. The TEM diffraction detects a period in basal plane stacking of 5. According to [14] these structures consist of two kinds of fragments which are different in the direction of the interlayer shift (ABCABC... and ACBACB...) with stacking faults among fragments. There are only three variants of stacking with period 5 which are denoted as (41), $(32)_3$, $(2111)_3$ in the Zhdanov notation

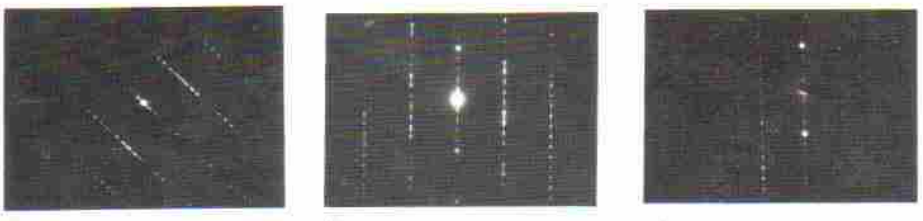

a) b) c)

Fig. 2a to c. Electron diffraction patterns of the θ phase in (a) $Ni_{45.1}Mn_{49.5}Ti_{5.4}$; (b) $Ni_{40.3}Mn_{51.9}Ti_{7.8}$; (c) $Ni_{40.5}Mn_{49.7}Ti_{9.8}$. Zone axes correspond to [110] of the fct lattice.

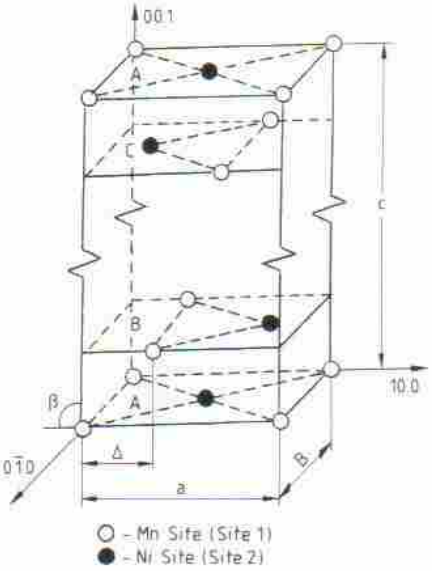

Fig. 3. Monoclinic unit cell of the θ' structure in NiMn(Ti) alloys. Three types of layers (A, B, C) can be packed in sequence depending on Ti content.

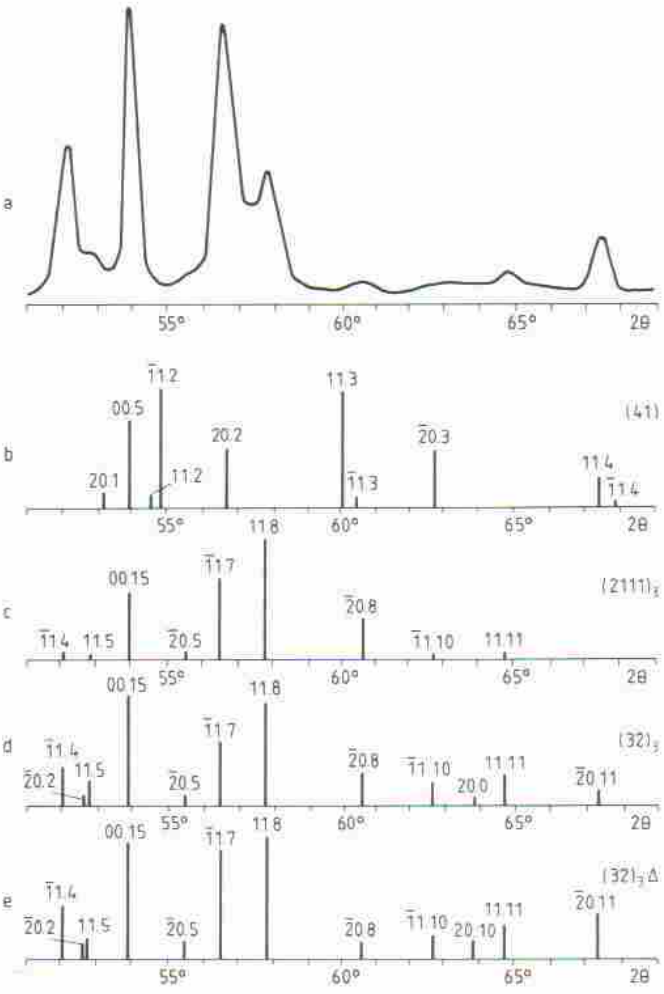

Fig. 4a to e. Experimental X-ray powder diffraction profiles of the θ' structure in (a) $Ni_{45.1}Mn_{45.0}Ti_{9.9}$ and calculated patterns for 5-layered stacking: (b) (41); (c) $(2111)_3$; (d) $(32)_3$. (e) A more accurate pattern for $(32)_3$ stacking with a shear value equal to $0.375a$.

[14], where the numbers in the brackets indicate the amount of layers in every fragment periodically repeating in the structure. The number 3 out of the brackets indicates that the respective sequence repeats 3 times in one unit cell. Calculated diffraction patterns for every variant as well as experimental profiles are represented in Fig. 4a to d. The best agreement with experimental data is seen for the $(32)_3$ variant. From the formal crystallographic point of view, the unit cell of the $(32)_3$ structure consists of 15 layers with stacking sequence ABCACBCABACABCB.... More careful analysis requires us to be taken into account that the Δ parameter (shift value between neighbouring layers) can deviate from $\frac{1}{3}a$ in ordered close packed structures. In fact, the X-ray study shows that the (31.15) peak in the vicinity of $2\theta = 132°$ is split. This indicates a small monoclinic distortion of the orthorhombic cell due to an irrational Δ value. In the case of the $(32)_3$ structure, the equation $\Delta = \frac{1}{3}a - \frac{1}{3}c \cdot \cos\beta$ follows from lattice geometry (see Fig. 3). Assuming $\beta = 90.9°$, Δ is $0.375a$ (in ordered close packed structures Δ deviates always from $\frac{1}{3}a$ because atomic sizes are different). The diffraction pattern of the $(32)_3$ structure corrected with the help of the Δ parameter is shown in Fig. 4e. An excellent agreement with the experimental profile can be seen.

A number of θ'-NiMn(Ti) structures were examined in this way. It has been found that the stacking sequence variation can be expressed as $(10)_3 \rightarrow (53)_3 \rightarrow (32)_3 \rightarrow (22)$ with Ti increasing from 0 to 15 % (Fig. 5). The $(53)_3$ and $(32)_3$ structures are weakly monoclinic, but (22) is a perfectly orthorhombic structure because opposite stacking faults balance each other. So the effect of Ti on the θ-NiMn structure can be summarized as follows: Ti addition leads to correlated stacking faults appearing at decreasing periodic distance as the Ti concentration increases.

4 Atomic and Magnetic Ordering

The transformation behaviour of Mn-based alloys is well known to depend strongly on interactions of magnetic moments localized on the manganese atoms [10]. In equiatomic NiMn, the structural $\beta \rightarrow \theta$ transformation is accompanied by long-range antiferromagnetic order in {001} planes of the θ phase [15]. It seems important to study what kind of magnetic structure should be obtained as a result of

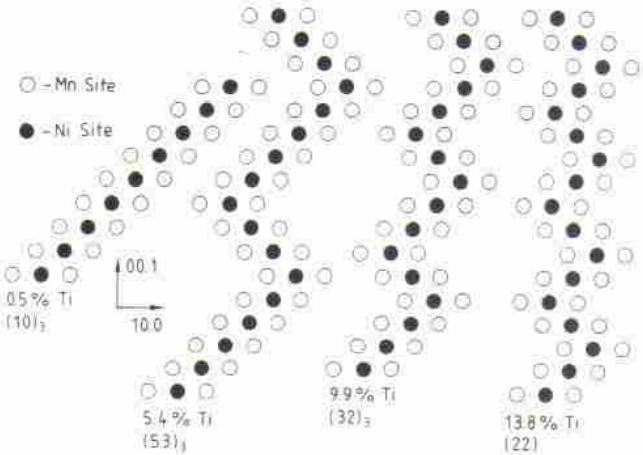

Fig. 5. The variation of stacking sequence with increasing Ti content. Projections on the 01.0 martensite plane are shown in monoclinic terms. The sequence is marked as $(10)_3$, $(53)_3$, $(32)_3$ and (22) in the Zdanov notation [14].

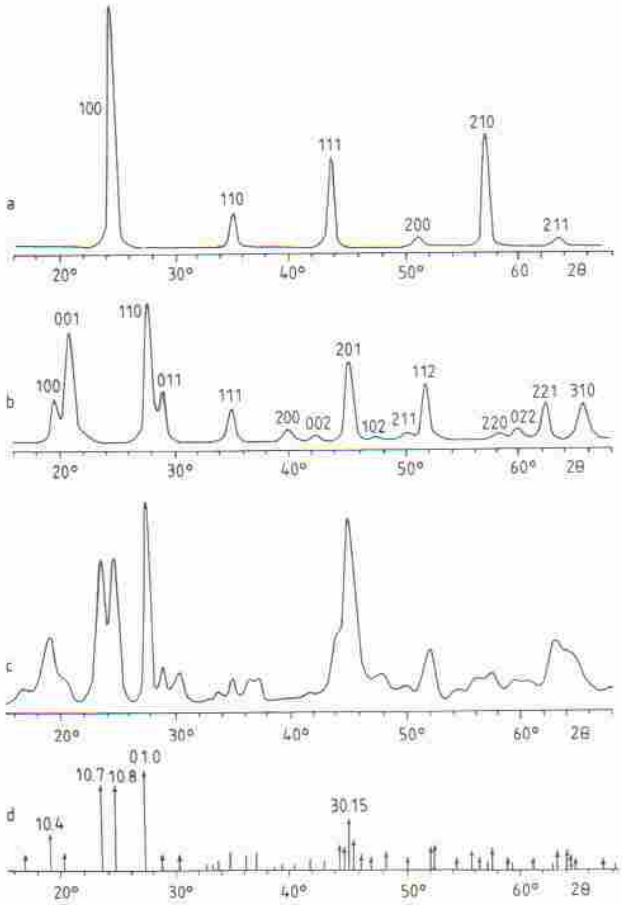

Fig. 6. Neutron powder diffraction of (a) the β phase in $Ni_{42.4}Mn_{43.8}Ti_{13.8}$; (b) $Ni_{49.4}Mn_{50.1}Ti_{0.5}$; (c) the θ' phase in $Ni_{45.1}Mn_{45.0}T_{9.9}$; (d) Calculated pattern for the θ' structure with $(32)_3$ stacking. The structural (fundamental) peaks are shown by lines and the superstructure peaks are shown by arrows. Only most intense peaks are indexed.

the structural change from θ to θ'. A comparison of the allotropic β, θ and θ' forms of NiMn(Ti) by neutron diffraction is appropriate. As the atomic scattering factor of Ni for neutrons is positive (+1.03) but those for Mn and Ti have a negative sign (−0.37 and −0.38, respectively) [16], superstructural reflections in ordered structures may be more intense than fundamental ones, and atomic and magnetic order parameters can be calculated with higher precision. Figure 6a shows a diffraction profile of β-NiMn(Ti) where strong (100), (111), (212) superstructural peaks and weak (110), (200) and (211) fundamental peaks are present. No magnetic peaks have been found.

The quantitative analysis of intensities, taking into account the appropriate structure and Lorentz polarisation factors, shows that atoms with negative atomic scattering factor occupy sites 1 (Mn sites), see (Fig. 3), and atoms with positive ones occupy sites 2 (Ni sites). The order parameters listed in Table 1 are near 1. It can be noticed that compositional disordering in alloys containing (Ti + Mn) > 50 % has not been observed. This may be due to vacancies present in Ni sites. So we have to conclude that Ti atoms occupy Mn sites in the NiMn lattice. This is not surprising in view of the strong interaction between Ti and Ni atoms in intermetallic compounds.

The neutron diffraction pattern of θ-NiMn containing 0.5 % Ti is similar to those of equiatomic NiMn reported in [15, 17] (Fig. 6b). In accordance with $L1_0$ ordering, intense superstructure reflections (001), (110), (201), (112), (221), (310) are observed. Also (100), (011), (102) magnetic reflections are present indicating long-range magnetic order which is believed to be the same as the layered antiferromagnetic type recognized in pure NiMn [17]. Using standard intensity analysis one can calculate the atomic order parameter to be about 1 and the magnetic moment on the Mn site to be $3.8 + 0.2\mu_B$, which are close to those in equiatomic NiMn.

Another situation has been observed in alloys containing about 10 % Ti which assume the θ' structure. Neutron diffraction shows a complicated profile which is certain to be a superposition of a number of lines (Fig. 6c). Weaker structural peaks are located in exact agreement with the θ' long-period structure described above (Fig. 6d). Also, the more intense superstructural peaks can be fully explained if it is assumed that the type of ordering in (00.1) basal planes is analogous to that in {111} basal planes of θ-NiMn as shown in Fig. 3. The calculated superstructural pattern, assuming that Mn sites are occupied occasionally by both Mn and Ti atoms and Ni sites are occupied by Ni, is indicated in Fig. 6d by arrows. A combination of fundamental and superstructural peaks results in good agreement with the experimental profile.

On the other hand, no additional magnetic peaks or magnetic contribution to superstructural peaks have been observed. This proves that in contrast to θ-NiMn(Ti) long-range magnetic order is absent in the alloys with θ' structure.

Thus, the change from the $\beta \Leftrightarrow \theta$ to the $\beta \Leftrightarrow \theta'$ type of transformation with increasing Ti content leads to a considerable change in magnetic interactions in Ni–Mn–Ti alloys. This is confirmed by magnetic susceptibility measurements on alloys with θ' or β structure at room temperature. In the β-alloys, the susceptibility shows a very complicated temperature dependence. For instance, the curve for $Mn_{42.4}Ni_{43.8}Ti_{13.8}$ can be divided into 3 different temperature ranges (I to III in Fig. 7). (I) From 15 to 200 K. In this range, the susceptibility exhibits a monotone increase with decreasing temperature and corresponding decrease without any hysteresis on heating. This behaviour is attributed to a paramagnetic phase with large negative

Table 1. Relation between (100) superstructural (F_{sup}) and (110) "structural" (fundamental) (F_{str}) diffraction lines of the β structure in NiMn(Ti) and calculated long-range order parameters of atomic order (s).

Mn at.%	Ni at.%	Ti at.%	F_{sup}/F_{str} experimental	F_{sup}/F_{str} calculated for $s = 1$	s calculated from experimental data
51.4	30.9	17.7	4.17	4.18	1.00
43.8	42.4	13.8	7.00	7.46	0.97
43.4	42.0	14.6	8.14	7.76	1.02

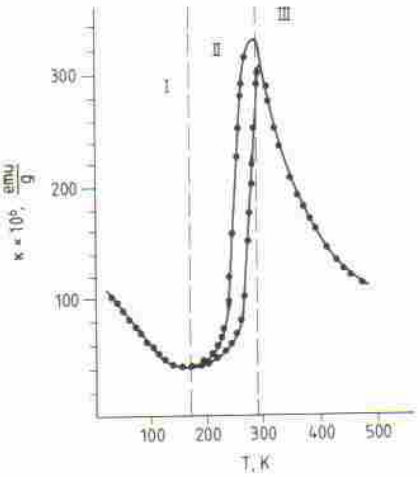

Fig. 7. The temperature dependence of magnetic susceptibility in $Ni_{42.4}Mn_{43.8}Ti_{13.8}$. Three regions correspond to θ' (I), θ' + β (II) and β (III) states.

exchange interaction. (II) From 200 to 300 K. In this range, a drop of susceptibility on cooling is observed. Comparing the cooling and heating curves, small hysteresis can be noticed. This kind of temperature dependence is attributed to materials undergoing a thermoelastic martensitic transformation. (III) Above 300 K. Heating leads to a decrease of susceptibility in accordance with a Curie-Weiss dependence. The obtained results prove that the β→θ' structural transformation in NiMn(Ti) alloys is accompanied by a change of the magnetic state change from strong paramagnetism (β phase) to weak paramagnetism with large negative exchange interaction (θ' phase). This conclusion can be supported by a calculation of the magnetic energy parameters for both phases on the basis of the reciprocal susceptibility as a function of temperature.

As mentioned previously, the temperature dependence of susceptibility in the β state is close to the Curie-Weiss law which allows to determine the magnetic interaction parameters: paramagnetic Curie temperature (T_c) and magnetic moment per atom in the β state (M). The calculation of the moment is possible if the number of atoms in which moments are located is known. In this case, Ni as well as Mn atoms may be magnetically active. Therefore we have examined two variants, [first, assuming that the magnetic moments are localized in manganese atoms only and, second, assuming that the moments located both in Mn and Ni atoms]. (It is impossible to distinguish these two variants by neutron scattering on polycrystals. This will be tested in the future on single crystals.) The calculated parameters are listed in Table 2. The β structure is seen to be strongly paramagnetic with relatively high T_c and large values of the magnetic moments. However, a pronounced drop of T_c and M is observed as a result of the β→θ' transformation. In the θ' state, the susceptibility may be described by the Curie-Weiss law, too, if the T_c value is accepted to be negative. This is in good agreement with the above supposition that the θ' phase is weakly paramagnetic with a large negative magnetic exchange interaction. It should be noted that the Curie-Weiss approach with negative T_c is also exactly correct for the alloys which exhibit the θ' structure at room temperature and above (up to 200 K).

It can be concluded that the parent β phase is strongly paramagnetic in the Ni–Mn–Ti system. The martensitic θ phase is a layered antiferromagnet and the martensitic θ' phase is weakly paramagnetic. Thus, the role of magnetic

Table 2. Magnetic interaction parameters in NiMn(Ti): paramagnetic Curie Point (T_c) and magnetic moment (h) per atom assuming that these are located on Mn atoms only (M_{Mn}) and both on Mn and Ni atoms (M_{Mn+Ni}).

Mn at.%	Ni at.%	Ti at.%	β			θ'				
			T_c K	M_{Mn} μ_B	M_{Mn+Ni} μ_B	T_c K	M_{Mn} μ_B	M_{Mn+Ni} μ_B	M_f K	A_f K
45.1	45.0	9.9	–	–	–	−72	1.99	1.41	358	522
42.4	43.8	13.8	200	5.29	3.71	−48	2.96	2.07	186	292

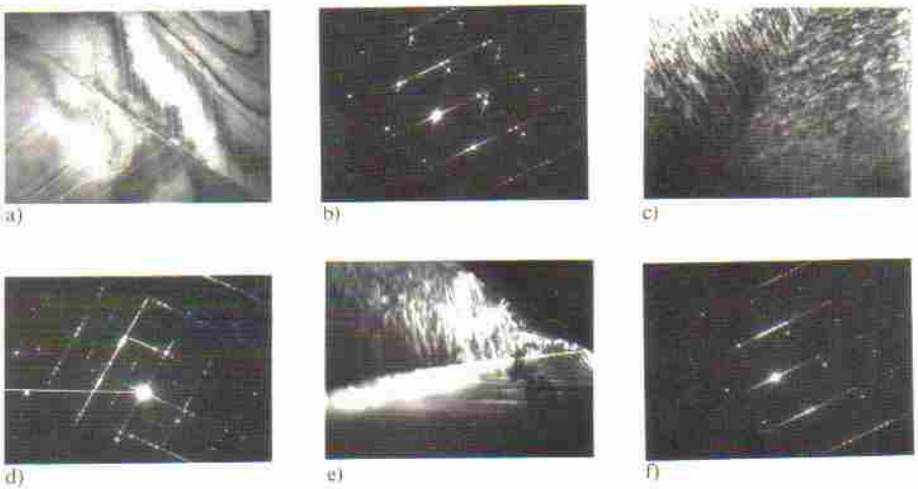

Fig. 8a to f. TEM micrographs showing the types of martensite coupling variants and corresponding diffraction patterns in $Ni_{45.1}Mn_{49.5}Ti_{5.4}$. (a) and (b) A/C. (c) and (d) A/D. (e) and (f) A/B.

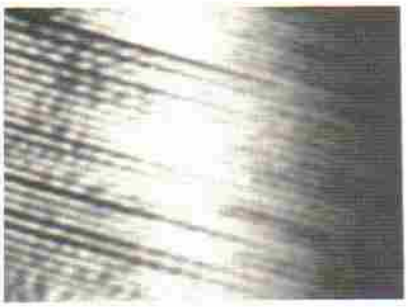

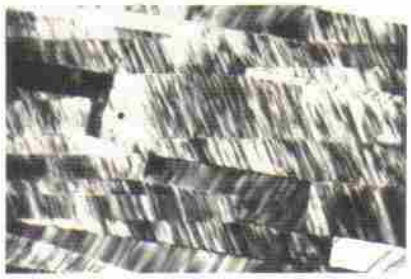

Fig. 9 (left). High resolution electron microscopy image showing periodic stacking faults inside martensite variant in $Ni_{46.8}Mn_{48.2}Ti_{5.0}$.

Fig. 10 (right). Mixed martensite microstructure in $Ni_{40.5}Mn_{49.7}Ti_{9.8}$.

interactions decreases when the $\beta \rightarrow \theta$ transformation is replaced by the $\beta \rightarrow \theta'$ one. In the latter case, the chemical interaction is clearly more important than the magnetic one.

5 Microstructure

The morphology of θ'-NiMn(Ti) has been studied by TEM. Typical micrographs and corresponding electron diffraction patterns which illustrate the features of the θ' martensitic phase in the alloys with $(53)_3$ structure are shown in Fig. 8. The microstructure is similar to that observed in the binary intermetallic compound NiMn by Adashi and Wayman [18]. The θ' martensite crystallites form three main coupling variants consisting of plates with habit planes parallel to the {011}, {100}, {155} parent planes. Every martensite crystal contains internal twins of high density with twinning planes {00.1} in monoclinic terms which correspond to {111} planes in fct terms. The above morphology is typical for alloys with a thermoelastic martensitic transformation [19].

Figure 9 shows a high resolution electron micrograph of one martensitic variant. We can see the irregular character in the distribution of stacking faults. This corresponds to the X-ray and electron diffraction patterns indicating a pronounced peak broadening in this alloy.

As in the case of the fct-$(53)_3$ structure transition, the variation from $(53)_3$ to $(32)_3$ structure is not accompanied by a change of martensite morphology. This allows us to conclude that the $(10)_3 \rightarrow (32)_3$ transition occurs as a result of stacking faults appearing in fct-martensite. Their density increases and the correlation in their location becomes more pronounced with increasing Ti concentration.

In contrast, the $(32)_3 \rightarrow (22)$ transition is not permanent and there is a concentration range where these phases can coexist. Figure 10 shows a mixture of martensitic phases possessing $(32)_3$ and (22) structures. In this case, martensitic crystallites of different types penetrate each other, and the morphology becomes far less regular.

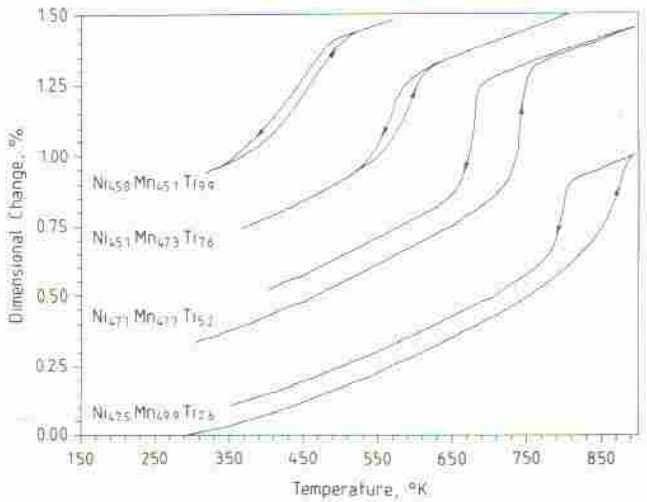

Fig. 11. Dilatometer curves of NiMn(Ti) alloys with various Ti content.

6 Transformation Temperatures

The transformation points in NiMn(Ti) were studied using dilatometry. Figure 11 shows typical dilatometer curves for the alloys with nearly equal Ni and Mn contents. The bending points can be identified with the transformation start and finish temperatures. In accordance with the X-ray examination mentioned in Sect. 3, transformation temperatures decrease with increasing Ti content. Also a permanent decrease of the thermal hysteresis from 60 K at 2.6 % Ti to 20 K at 9.9 % Ti was observed. The hysteresis of 10 to 40 K is attributed to the establishment of thermoelastic equilibrium between martensitic and parent phases during shear transformation. This fact, combined with microstructural results reported in Sect. 5, allows us to suggest that the $\beta \rightarrow \theta'$ transformation is a thermoelastic one, at least in the alloys containing 7.6 to 9.9% Ti, and we can use the estimation of the equilibrium temperature T_0 between martensite and parent phases established by Tong and Wayman [20]: $T_0 = (M_s + A_f)/2$. The values of transformation temperatures, thermal hysteresis and estimated T_0 are listed in Table 3.

It is known for Hume-Rothery β phases that the stability of the bcc structure is a function of the electron concentration per atom (see, e.g. [21]). In the NiMn(Ti) case, the equilibrium temperature exhibits a linear dependence on the $(s + d)$ electron concentration (Fig. 12). An extrapolation to e/atom = 8.5 gives a value $T_0 = 990$ K which agrees with the data concerning β phase stability in equiatomic NiMn [22]. Also shown in this figure are the T_0 values calculated from experimental data obtained for binary nonstoichiometric NiMn [11] and ternary NiMn(Al) [23]. It is seen that all T_0 values for NiMn-based alloys can be fitted by one linear dependence in the range of 8.20 to 8.52 e/atom. At values below 8.20 e/atom, deviations between NiMn(Ti) and NiMn(Al) have been observed. This is related to the special electronic structure of nonstoichometric NiMn and is a problem to be clarified by band structure calculation in future.

Table 3. Transformation temperatures M_s, M_f and thermal hysteresis A_s, A_f, and estimated equilibrium temperature T_0 between β and θ' structures in NiMn(Ti).

Mn at.%	Ni at.%	Ti at.%	Phases at 293 K	M_s K	M_f K	A_s K	A_f K	T_0 K	Hysteresis K
49.9	47.5	2.6	θ'	820	770	820	895	855	56
45.3	49.9	4.8	θ'	800	695	775	855	830	58
47.7	47.1	5.2	θ'	695	655	715	760	725	60
47.3	45.1	7.6	θ'	600	535	555	620	610	20
45.1	45.0	9.9	θ'	495	355	385	525	510	18
42.4	43.8	13.8	β	275	190	205	295	285	23
52.1	45.3	2.6	θ' + γ	775	735	815	840	805	70
54.4	40.8	4.8	θ' + γ	565	520	565	620	590	45
51.8	43.0	5.2	θ' + γ	635	605	650	695	665	61
49.5	45.1	5.4	θ' + γ	670	605	680	745	705	63
50.0	42.5	7.5	θ' + γ	520	475	505	550	535	29
54.5	37.9	7.6	θ' + γ	410	355	390	445	420	23
51.9	40.3	7.8	θ' + γ	495	445	475	515	505	22
47.8	42.7	9.5	θ' + γ	455	375	415	480	465	28
49.7	40.5	9.8	θ' + γ	345	305	330	370	355	28

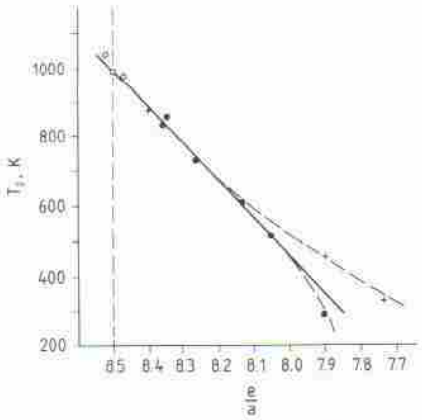

Fig. 12. The $(s+d)$-electron concentration (e/atom) dependence on T for NiMn-based alloys: ● NiMn(Ti), ○ nonstoichiometric NiMn [11], + NiMn(Al) [23].

7 Concluding Remarks

The data and their analysis reported above allow us to make some conclusions about the mechanism of structural transformation in binary and ternary NiMn-based alloys.

Ti addition in small concentrations induces stacking faults which are weakly spatially correlated. Increasing Ti content leads to an increase of the stacking fault density and stronger correlation among them. As a result, the lattice loses the initial $L1_0$ symmetry and long period structures are observed. A similar situation is likely for NiMn with Al addition [11] and in Mn-rich NiMn [24] alloys.

Corresponding to the structural variation, the magnetic state is changing from antiferromagnetism in the θ structure to weak paramagnetism in the θ' structure. Following a widespread point of view, the driving force for the transformation in Mn-containing intermetallic compounds is the ordering of magnetic moments localized on Mn atoms. A structural transformation from cubic to tetragonal phase is considered to be a result of the magnetic transformation. However, our data contradict this view because we deal with the $\beta \rightarrow \theta'$ transformation which is not accomplished by a significant change in the magnetic state. Therefore, it seems that the structural transformation in NiMn takes place first, and long-range magnetic ordering takes place in the tetragonal structure only. This is in agreement with the latest NiMn band structure calculation [25]. It was shown that the $\beta \rightarrow \theta$ transformation is close to a classic Zener transition from a soft structure with high frequency entropy to a low-energy close packed structure.

The sharp suppression of antiferromagnetism can be related to the high density of correlated stacking faults. The magnetic structure in equiatomic NiMn is known to consist of Ni and Mn layers with antiferromagnetic coupling within the Mn layers (Fig. 13). As the basal planes are tilted by angles of about 55° from the Mn layers, stacking faults destroy the antiferromagnetic layers. We suppose that the magnetic ordering disappears mainly for this reason. Additionally, some effect of the nonmagnetic Ti atoms on the magnetic exchange interaction and on the soft distance of magnetic order cannot be excluded.

The existing opinion that the magnetostructural transformation in the NiMn intermetallic compound is close to those in the disordered Mn-based alloys (Mn–Ni, Mn–Cu, Mn–Ga, Mn–Ge) is evidently wrong. The transformation in NiMn is rather similar to that in CuZn, AuCd, NiTi, NiAl. This corresponds well to the known thermoelastic transformation behaviour in the NiMn-based alloys. A favourable condition for thermoelasticity is known to be a high degree of atomic order in the parent and martensitic phases. High values of the long-range order parameters were found in NiMn(Ti).

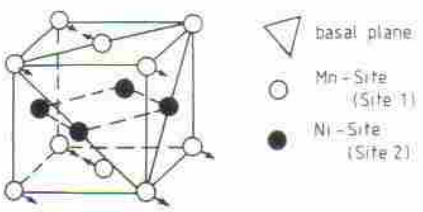

Fig. 13. Magnetic NiMn structure according to [17]. Magnetic moments are indicated by arrows.

Literature

1. *Kurdjumov, G. V.; Khandros, L. G.:* Dokl. USSR Academy of Sciences *66* (1949) 211–214.
2. *Warlimont, H.; Delaey, L.:* Martensitic Transformation in Copper–Silver and Gold-based Alloys, Pergamon Press, Oxford (1974).
3. *Miuazaki, S.; Otsuka, K.:* ISIJ International *29* (1989) 353–377.
4. *Chakravorty, S.; Wayman, C. M.:* Metall. Trans. A *7A* (1975) 555–582.
5. *Brun, K.; Kjekshus, A.; Pearson, W. B.:* Phil. Mag. *10* (1964) 291–299.
6. *Brun, K.; Kjekshus, A.; Pearson, W. B.:* Acta Chem. Scand. *19* (1965) 107–112.
7. *Pearson, W. B.; Brun, K.; Kjekshus, A.:* Acta Chem. Scand. *19* (1965) 477–484.
8. *Morris, D. P.; Morris, J. G.:* Acta metall. *26* (1978) 547–555.
9. *Kren, E.; Soluom, J.:* Phys. Lett. *22* (1966) 273–274.
10. *Vintaykin, E. Z.; Udovenko, V. A.:* Izvestia Vusov *No5* (1985) 104–117.
11. *Adashi, K.; Wayman, C. M.:* Metall. Trans. A *16A* (1984) 1567–1579.
12. *Vintaykin, E. Z.; Mackushev, S. Yu.; Polyakova, N. A.; Potapov, P. L.; Udovenko, V. A.:* Fiz. Metall. Metalloved. *No6* (1990) 115–120.
13. *Smithells, K. I. (ed.):* Metals Reference Book, Butterworths and Co., London/Boston (1976).
14. *Zhdanov, G. S.:* Dokl. USSR Academy of Sciences *48* (1949) 40–43.
15. *Kasper, J. S.; Kouvel, J. S.:* J. Chem. Solids *11* (1959) 231–238.
16. *Bacon, J. E.:* Neutron Diffraction, Clarendon Press, Oxford (1956).
17. *Vintaykin, E. Z.; Dmitriev, V. D.; Mackushev, S. Yu.; Udovenko, V. A.:* Fiz. Metall. Metalloved. *63* (1987) 577–581.
18. *Adashi, K.; Wayman, C. M.:* Metall. Trans. A *16A* (1984) 1581–1597.
19. *Saburi, T.; Wayman, C. M.:* Acta metall. *27* (1979) 979–995.
20. *Tong, H. C.; Wayman, C. M.:* Acta metall. *22* (1974) 887–896.
21. *Zungwill, A.; Bruinsma, R.:* Comments Cond. Mat. Phys. *13* (1987) 1–19.
22. *Kren, E.; Nagy, E.; Pal, L.:* Phys. Chem. Solids *29* (1968) 101–108.
23. *Henninger, F.; Opielka, H.; Wachtel, E.:* Z. Metallkd. *77* (1986) 747–748.
24. *Baele, I.; van Tendeloo, G.; Amelinckx, S.:* Acta metall. *35* (1987) 401–412.
25. *Bashirov, V. Z.; Velikokhyrtny, O. I.; Demidenko, V. S.; Naumov, I. I.:* Fiz. Metall. Metalloved. *No9* (1992) 12–16.

(Received July 20, 1994)